

**1 Gassmann fluid substitution and shear modulus variability in carbonates**  
**2 at laboratory seismic and ultrasonic frequencies**

**3 Ludmila Adam<sup>1</sup>, Michael Batzle<sup>1</sup>, and Ivar Brevik<sup>2</sup>**

**4**

**5 ABSTRACT**

**6** Carbonates have become important targets for rock property  
**7** research in recent years because they represent many of  
**8** the major oil and gas reservoirs in the world. Some are under-  
**9** going enhanced oil recovery. Most laboratory studies to un-  
**10** derstand fluid and pressure effects on reservoir rocks have  
**11** been performed on sandstones, but applying relations devel-  
**12** oped for sandstones to carbonates is problematic, at best. We  
**13** measured in the laboratory nine carbonate samples from the  
**14** same reservoir at seismic (3 to 3000 Hz) and ultrasonic  
**15** (0.8 MHz) frequencies. Samples were measured dry (humid-  
**16** ified), and saturated with liquid butane and brine. Our car-  
**17** bonate samples showed typical changes in moduli as a func-  
**18** tion of porosity and fluid saturation. However, we explored  
**19** the applicability of Gassmann's theory on limestone and dol-  
**20** omite rocks in the context of shear and bulk modulus disper-  
**21** sion, and Gassmann's theory assumptions. For our carbonate  
**22** set, at high differential pressures and seismic frequencies, the  
**23** bulk modulus of rocks with high aspect ratio pores and dol-  
**24**omite mineralogy is predicted by Gassmann's relation. We  
**25** also explored in detail some of the assumptions of Gas-  
**26**smann's relation, especially rock-frame sensitivity to fluid  
**27** saturation. Our carbonate samples showed rock shear-modu-  
**28**lus change from dry to brine saturation conditions, and we in-  
**29**vestigated several rock-fluid mechanisms responsible for this  
**30**change. To our knowledge, these are the first controlled labo-  
**31**ratory experiments on carbonates in the seismic frequency  
**32**range.  
**33**

used relations to estimate the effect of fluids on bulk modulus is **37**  
Gassmann's fluid substitution theory (Gassmann, 1951), which we **38**  
will examine in the following section. Laboratory measurements on **39**  
carbonates have been performed at ultrasonic frequencies (~0.8 **40**  
MHz) to estimate the validity of Gassmann's equations for lime- **41**  
stones and dolomites (Wang et al., 1991; Marion and Jizba, 1997; **42**  
Wang, 2000; Baechle et al., 2005; Røgen et al., 2005). In most **43**  
cases Gassmann's predictions underestimate the observed ultra- **44**  
sonic velocities for either oil- or brine-saturated samples, al- **45**  
though for some samples Gassmann theory overestimates the **46**  
measured velocities (Wang, 2000; Baechle et al., 2005; Røgen et **47**  
al., 2005). **48**

Presently, the applicability of Gassmann's equation to carbonate **49**  
rocks is unresolved. With our work, we hope to make inferences **50**  
about the uncertainties and interpretation on the applicability of **51**  
Gassmann's equation. Our work focuses on understanding the appli- **52**  
cability of Gassmann's fluid substitution theory at seismic and ultra- **53**  
sonic frequencies. We also analyze the validity of some of the as- **54**  
sumptions for Gassmann's theory, especially rock-frame sensitivity **55**  
to fluids. Our carbonate samples consist of different fabrics, mineral- **56**  
ogies, porosities, and permeabilities; still we must be careful in gen- **57**  
eralizing our results to all carbonate reservoirs. **58**

First, we present Gassmann's theory and its assumptions. Second, **59**  
we describe the laboratory acquisition, processing, and data uncer- **60**  
tainty analysis at seismic and ultrasonic frequencies. Then, we intro- **61**  
duce shear modulus variability with fluid substitution and the possi- **62**  
ble mechanisms that could explain these changes. Finally we com- **63**  
pare our measured bulk modulus to Gassmann's predictions for **64**  
these carbonate rocks. **65**

**34 INTRODUCTION**

**35** An important area of research for carbonate rocks is the fluid sub-  
**36**stitution effect on elastic moduli and velocities. One of the widely

**GASSMANN'S EQUATION** **66**

Gassmann's fluid substitution relation is commonly applied to **67**  
predict the bulk modulus for rocks saturated with different fluids: **68**

Manuscript received by the Editor April 18, 2006; revised manuscript received June 29, 2006.  
<sup>1</sup>Colorado School of Mines, Center for Rock Abuse, Department of Geophysics, 1500 Illinois Street, Golden, Colorado 80401. E-mail: ladam@mines.edu; mbatzle@mines.edu.  
<sup>2</sup>Statoil Research Centre, Posttuttak, N7500 Trondheim, Norway. E-mail: ivb@statoil.com.  
© 2006 Society of Exploration Geophysicists. All rights reserved.

$$K_{sat} = K_{dry} + \frac{\left(1 - \frac{K_{dry}}{K_{min}}\right)^2}{\frac{\phi}{K_{fl}} + \frac{1 - \phi}{K_{min}} - \frac{K_{dry}}{K_{min}^2}} \quad (1)$$

69

70 Gassmann's equation 1 estimates the saturated bulk modulus ( $K_{sat}$ )  
 71 through the bulk modulus of the forming minerals ( $K_{min}$ ), the bulk  
 72 modulus of the frame or dry rock ( $K_{dry}$ ), the bulk modulus of the fluid  
 73 ( $K_{fl}$ ), and the rock porosity ( $\phi$ ) (Gassmann, 1951). Note that in Gas-  
 74 smann's relation, the considered property of the fluid in the rock is  
 75 only the fluid bulk modulus.

76 Gassmann's derivation is based on the following assumptions for  
 77 a porous system: (1) Pore pressure is in equilibrium between pores.  
 78 This can be achieved at very low frequencies, usually at seismic fre-  
 79 quencies or lower, where the fluid has enough time to reach relax-  
 80 ation or equilibrium. However, the relaxation time depends also on  
 81 fluid viscosity and density, and rock permeability. (2) The porous  
 82 frame consists of a single solid material (monomineralic). (3) Pores  
 83 are in flow communication and are homogeneously, fully filled with  
 84 a nonviscous fluid. (4) The system is closed (undrained). (5) The  
 85 pore fluid does not chemically influence the solid frame. Although  
 86 implied, a constant rock shear modulus from dry to any fluid-type  
 87 saturation is not an assumption but an outcome of Gassmann's theo-  
 88 ry (Berryman, 1999).

89 The beauty of equation 1 is its simplicity as well as the fact that the  
 90 variables have physical significance and are usually well con-  
 91 strained or can be directly measured. Other fluid substitution theo-  
 92 ries require the knowledge of such factors as the symmetry of the  
 93 rock, the geometry of the inclusions, and the crack density among  
 94 others. For example, in the low-frequency limit, where no pore-pres-  
 95 sure gradients exist, Brown and Korringa (1975) relate the aniso-  
 96 tropic rock effective elastic compliance tensor to the same rock filled  
 97 with fluid, and for an isotropic and monomineralic rock, their rela-  
 98 tions reduce to Gassmann's equation. For this fluid-substitution theo-  
 99 ry, knowledge of the anisotropic symmetry and pore-space compres-  
 100 sibility are required. Other fluid substitution theories mostly  
 101 assume isolated inclusions and their geometries in the derivation of  
 102 the equations. Isolated cavities should then also be isolated with re-  
 103 spect to fluid flow (presence of pore-pressure gradients). Therefore,  
 104 theories that assume isolated inclusions (Kuster and Toksoz, 1974;

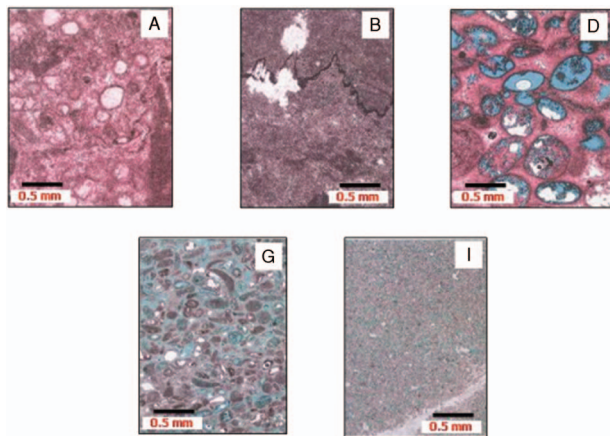


Figure 1. Thin sections for some of our carbonate samples. Pink represents calcite, gray dolomite, white anhydrite and blue pore space.

O'Connell and Budiansky, 1974; Hudson, 1981) may be more appli-  
 cable to the high-frequency range and require knowledge of param-  
 eters related to pore space.

CARBONATE SAMPLES

Our carbonates are from two wells in a single reservoir with  
 depths between 2915 and 3180 m below sea level. The reservoir has  
 lagoon, ramp and shoal depositional environments. These different  
 depositional systems create different textures, porosities and perme-  
 abilities (Figure 1). Some reservoir regions have been dolomitized.  
 Dolomitization is evident from high porosity and high permeability  
 because dissolved grains or fossils become pore space, increasing  
 the connectivity between pores, thus increasing permeability. The  
 reservoir is not fractured and has few clay minerals, but does have  
 minor anhydrite. The available samples comprise nine carbonates  
 with varying porosity (5%–35%), permeability (0.001–800 mD),  
 mineralogy (dolomite and limestone), and texture. The samples are  
 either almost pure calcite or dolomite (95% total volume) with less  
 than 3% clays and 5% anhydrite of total volume. Samples with large  
 anisotropy or vuggy pores are avoided. Table 1 summarizes the pet-  
 rological data for our samples. Porosity and permeability are mea-  
 sured using standard helium porosimetry and air permeability equip-  
 ment at atmospheric pressure. Permeability values are corrected for  
 Klinkenberg gas slippage. The samples are cylindrical, 3.75 cm in  
 diameter and 3.75 to 5 cm in length.

Velocity and elastic modulus data are acquired at nine pressure  
 points. Confining pressure varies from 3.5 to 34.5 MPa while pore  
 pressure is held constant at 3.5 MPa, thus reaching a maximum dif-  
 ferential pressure of 31 MPa. The low-frequency system in the labo-  
 ratory is pressurized with nitrogen gas, but for safety reasons the sys-  
 tem is not able to reach the reservoir differential pressure  
 (34.5 MPa). Samples are measured dry, under butane ( $C_4H_{10}$ ), and  
 brine (200,000 ppm NaCl) saturations. Butane, at 3.5 MPa, is in  
 liquid state. Samples are measured with some amount of moisture  
 because even less than 1% of water can reduce the bulk and shear  
 moduli significantly (Clark et al., 1984). Because samples show sen-  
 sitivity to water, several are kept in a high-humidity chamber to pro-  
 vide an initial brine saturation (less than 1%). Samples A, C, E, F and  
 G are humidified previous to measurements, thus *dry* for these sam-  
 ples means humidified. Samples B, D, H and I are measured at room  
 conditions (30% humidity). Samples are coated with a thin, imper-  
 meable polyimide film (Kapton), over which strain gauges are glued  
 to measure rock deformations at seismic frequencies. This film  
 keeps the moisture inside the rock and prevents nitrogen diffusion.

DATA EXAMPLE: ACQUISITION AND PROCESSING

Samples are measured at low (seismic: 3–3000 Hz) and ultrason-  
 ic frequencies (~0.8 MHz), although sample G is measured at ul-  
 trasonic frequencies only. Seismic frequency moduli and velocities  
 are derived from the strain-stress method (Spencer, 1981; Batzle et  
 al., 2006). Measured strains on the rock and a calibrating material  
 (aluminum) are converted into Young's modulus and Poisson's ratio,  
 and from these we get bulk and shear moduli. Batzle et al. (2006)  
 give a detailed description of the apparatus and the estimation of  
 elastic moduli from measured strains. In the stress-strain experi-  
 ment, we directly estimate the bulk and shear moduli. Thus, our  
 moduli estimates are independent of the rock density. As we will see,

161 for ultrasonic data the rock density *is* needed to estimate the bulk and  
162 shear moduli.

163 For ultrasonic data, we measure the time a wave takes to propa-  
164 gate from the top of the sample to the bottom (Birch, 1960). The ve-  
165 locity, either P- or S-wave, is estimated by:  $V = (L - \delta L)/(T_m - T_0)$ ,  
166 where  $L$  is the sample length measured at atmospheric pressure,  $\delta L$  is  
167 the change in sample length due to pressurization,  $T_m$  is the measured  
168 travel time, and  $T_0$  is a time correction.  $\delta L$  is ignored because the  
169 change in length, which we can estimate from the low-frequency ex-  
170 periment, is very small.  $T_0$ , the travel time through the aluminum  
171 material between the ultrasonic transducer and the sample, is known  
172 and constant for all measured samples. Therefore, we can rewrite the  
173 velocity as simply:  $V = L/T$ , where  $T$  is the corrected travel time. As-  
174 suming isotropy, the measured velocities and densities are then used  
175 to derive the shear and bulk moduli.

176 As an example of the estimated bulk modulus over the entire fre-  
177 quency range, we show results for sample *H* in Figure 2. The compu-  
178 tation of the error bars and the linear fit are discussed later in this sec-  
179 tion. Observe that the rock bulk modulus increases with saturating  
180 fluid. However, the change in rock bulk modulus from dry to butane  
181 saturated is small compared to when the rock is saturated with brine.  
182 This is because butane has a lower fluid bulk modulus than brine.  
183 Figure 2 also shows bulk modulus dispersion (higher frequencies  
184 have a larger modulus). Several theories exist to explain the nature of  
185 this dispersion. A primary cause for dispersion can be pore-pressure  
186 disequilibrium caused by nonzero pore-pressure gradients. This un-  
187 relaxed pressure is described by several mechanisms: grain-fluid in-  
188 erial and viscous coupling (Biot, 1956), patchy saturation (White,  
189 1975; Dutta and Ode, 1979) and squirt or local fluid flow (Mavko  
190 and Jizba, 1991), among others. Our goal here is not to decide which  
191 of frequency dependent modulus or velocity theories are causing the  
192 dispersion. We do want to point out differences in modulus estimates  
193 as a result of the dispersion from seismic to ultrasonic frequencies.  
194 As previously mentioned, Gassmann's theory is the low-frequency  
195 limit, meaning that this theory may not be suitable to predict ultra-  
196 sonic data because of possible dispersion in the elastic moduli and  
197 velocities. Wang (1997), Marion and Jizba (1997), Baechle et al.  
198 (2005) and Røgen et al., 2005 have shown how, in most cases, Gas-  
199 smann's theory underpredicts ultrasonic frequency measurements.

200 Pore pressure can equilibrate if there is enough time for the fluids to  
201 relax. This means there is a characteristic frequency,  $f_c$  of the rock  
202 perturbation. For measurements acquired at a frequency less than  $f_c$ ,  
203 the pore pressure has reached equilibrium, while for higher frequen-  
204 cies than the  $f_c$ , pore fluids are not equilibrated, producing higher  
205 values for modulus and velocity.

206 Differential pressure also controls the modulus dispersion of a  
207 rock. At low-differential pressures where compliant pores or cracks  
208 are open, pore-pressure disequilibrium is more likely to occur. Wang  
209 (2000) shows, in a compilation of ultrasonic laboratory data of car-  
210 bonate samples, that Gassmann's theory substantially (up to 30%)  
211 underpredicts the measured velocities at low-differential pressures.  
212 At high-differential pressures, compliant pores close, and Gas-  
213 smann's theory predicts the measured data within 10%.

214 Carbonates are heterogeneous and vugs or moldic structures can  
215 have comparable length to the ultrasonic wavelength (0.5 cm for a  
216 wave at 0.8 MHz and with a velocity of 4500 m/s). Some of our  
217 samples showed inclusions of different densities or voids with di-  
218 mensions on the order of ultrasonic wavelengths. Therefore, scatter-  
219 ing of ultrasonic waves is possible in carbonate samples, especially  
220 in dry rocks where the density contrast between voids and the matrix  
221 is large. When scattered, the wave loses energy to multiple reflec-  
222 tions from grains, mostly resulting in lower moduli and velocities at  
223 higher frequencies. The larger modulus contrast will be for air-grain  
224 and butane-grain interfaces.

### Poisson's ratio: a correction

225 Samples *B*, *F* and *I* show higher values of Poisson's ratio at low  
226 frequency than expected in carbonates. Rock heterogeneity is proba-  
227 bly not the cause, since placing the strain gauges on large heteroge-  
228 neities (visible to the eye) on measured core plugs are avoided. The  
229 observed larger deformations of the sample in the horizontal direc-  
230 tion probably result from end effects in our stress-strain system. This  
231 large deformation or bulging can result from the combination of in-  
232 trinsically large Poisson's ratios in carbonates ( $>0.25$ ) and short  
233 samples (our sample length is close to its diameter). This bulging has  
234 been confirmed with preliminary finite-element modeling at our lab-  
235 oratory. Poisson's ratio depends on the  $V_p/V_s$ , but because the dis-  
236

**Table 1. Petrological data for the carbonate set. Mineralogy was obtained from XRD analysis and are reported in percent per volume (samples E, G and H had no XRD analysis). Mineral bulk modulus is computed using Voigt-Reuss-Hill average. Texture follows modified Dunham's carbonate classification (Moore, 2001): mud=mudstone, wacke=wackestone, pack=packstone, grain=grainstone, and bound=boundstone.**

| SAMPLES                             | A     | B     | C     | D     | E     | F     | G     | H      | I      |
|-------------------------------------|-------|-------|-------|-------|-------|-------|-------|--------|--------|
| Porosity                            | 1.6   | 4.6   | 21.0  | 24.9  | 28.5  | 34    | 23.6  | 29.6   | 34.7   |
| Permeability (mD)                   | 0.03  | 0.03  | 5.50  | 1.20  | 0.43  | 0.31  | 25.00 | 103.00 | 432.00 |
| Grain density (gm/cm <sup>3</sup> ) | 2.73  | 2.84  | 2.70  | 2.71  | 2.70  | 2.69  | 2.84  | 2.80   | 2.86   |
| Calcite (%)                         | 83.0  | 0.7   | 76.0  | 99.6  | –     | 97.0  | –     | –      | 0.4    |
| Dolomite (%)                        | 11.0  | 97.0  | 21.0  | 0.0   | –     | 0.0   | –     | –      | 93.0   |
| Anhydrite (%)                       | 0.5   | 0.5   | 0.0   | 0.0   | –     | 0.7   | –     | –      | 4.9    |
| Phyllosilicates (%)                 | 3.4   | 0.8   | 2.4   | 0.0   | –     | 2.3   | –     | –      | 1.1    |
| Quartz (%)                          | 0.6   | 0.6   | 1.2   | 0.4   | –     | 0.2   | –     | –      | 0.8    |
| K-feldspar (%)                      | 2.0   | 0.0   | 0.0   | 0.0   | –     | 0.0   | –     | –      | 0.0    |
| Mineral bulk modulus (GPa)          | 70.70 | 78.96 | 71.59 | 71.26 | 71.59 | 70.35 | 85.00 | 78.96  | 77.67  |
| Texture                             | Wacke | Mud   | Grain | Grain | Grain | Bound | Pack  | Wacke  | Mud    |

237 person in  $V_p$  and  $V_s$  are similar for our samples, the resulting disper-  
 238 sion in Poisson's ratio is negligible, making it possible to correct the  
 239 low-frequency data with the estimates we obtain from ultrasonic  
 240 data. Domenico (1984), Anselmetti and Eberli (1993), Mavko et al.  
 241 (1998), Assefa et al. (2003), and Han (2004, Fluids and DHI Consor-  
 242 tia Meeting Report) measured carbonate samples ultrasonically and  
 243 derived empirical relations for  $V_p$  and  $V_s$ . We use their relations to  
 244 compute Poisson's ratio for water/brine saturated carbonates and  
 245 compare their values to our samples' Poisson's ratios measured at ul-  
 246 trasonic frequencies (Figure 3). Agreement between modeled Pois-  
 247 son's ratio and our measurements lets us use the ultrasonic values to  
 248 correct the Poisson's low-frequency data. The correction consists of  
 249 multiplying the seismic frequency Poisson's ratio by a factor less  
 250 than one. This factor is obtained from the ratio of the ultrasonic and  
 251 the biased seismic frequency Poisson's ratios.

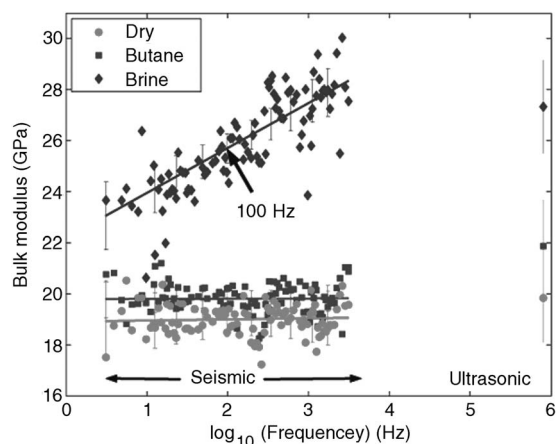


Figure 2. Seismic and ultrasonic frequency bulk modulus least-squares estimates (solid lines) and measured data for sample  $H$  at 31 MPa. Observe the modulus dispersion for different fluids. Error bars are two standard deviations of the estimated bulk modulus.

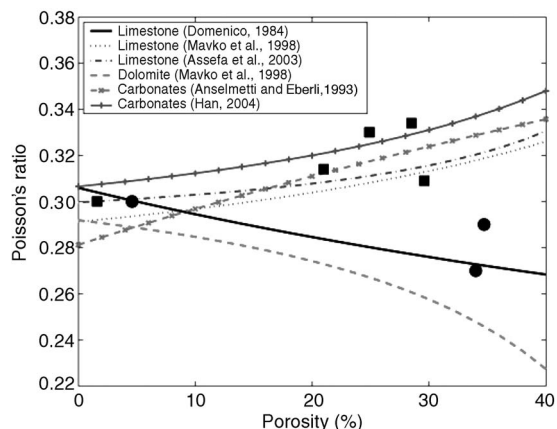


Figure 3. Modeled Poisson's ratio from empirical relations from ultrasonic data for carbonate rocks saturated with water/brine. Squares and circles are the Poisson's ratio obtained from our measurements at ultrasonic frequencies. This plot shows that our values of Poisson's ratio are in agreement with the empirical equations. Therefore, we use the ultrasonic Poisson's value to correct the low-frequency data for three of our samples ( $B$ ,  $F$  and  $I$ ) represented by circles.

Uncertainty analysis

Our data set consists of Poisson's ratio and Young's modulus as a function of frequency and differential pressure (seismic frequency), and travel time as a function of differential pressure (ultrasonic frequency). We assume that the Poisson's ratio and Young's modulus relation to the logarithm base 10 of frequency is linear, while the travel time with differential pressure follows a second order polynomial (*true* models). We also assume that the error between our data and these *true* models is random, Gaussianly distributed and with zero mean. Our core analysis is performed under the assumption that all requirements for Gassmann's theory applicability are satisfied. If our samples and experimental setup violate one (or more) of the assumptions of Gassmann's theory, we introduce a bias (systematic error) in our estimates, and we will give an interpretation to why some results on the samples do not obey Gassmann's assumptions.

Stress-strain methodology

In Figure 4 we plot data for the stress-strain experiment ( $E$  and  $\nu$ ) showing a linear trend with  $\log_{10}$  of frequency. We fit a straight line to our data and estimate the variance of our random error. We use the variance of the random error to compute the error of estimates of Young's modulus and Poisson's ratio, and later propagate this error into the estimates of bulk and shear moduli. Young's modulus of aluminum equals 70 GPa (needed to compute the rock Young's modulus), and we assume this value is error-free for the uncertainty analysis. On average, our estimates of the standard deviation of the estimated bulk modulus is 1.2 GPa, and that of the shear modulus is 0.3 GPa for seismic frequencies.

Ultrasonic pulse propagation

In addition to low frequency measurements, we have travel times at 0.8 MHz versus differential pressure. Travel time decreases with increasing differential pressure (higher velocity). Figure 5 shows this dependence, resulting from open cracks and compliant pores at low-differential pressures. A second order polynomial is fit to the ultrasonic travel time data as a function of pressure (dashed and solid lines in Figure 5), and we obtain the variance of the random error. We then compute the error of our estimated travel times.

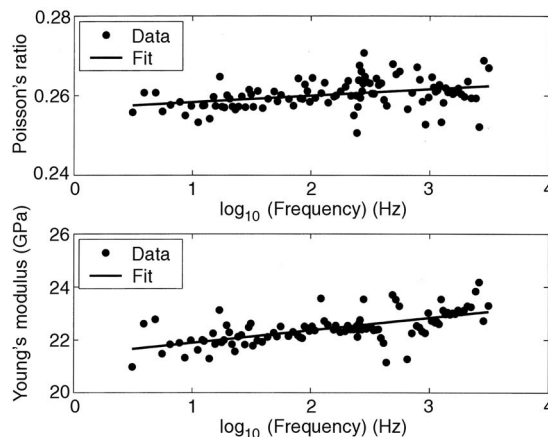


Figure 4. Error analysis on sample  $C$  at a differential pressure of 17.5 MPa and butane saturation. From the least-squares fit we estimate the variance in our estimate of  $E$  and  $\nu$ .

288 The ends of our samples are machine flattened and when the  
 289 length is measured repeatedly, no significant variability is observed,  
 290 so we consider that the length is error-free. We also assume there is  
 291 no error in the differential pressure measurements. Therefore, we  
 292 propagate only the estimated travel-time error into the P- and  
 293 S-wave velocity. Now, to estimate the bulk and shear moduli, we  
 294 need the rock density which depends on porosity, grain density, and  
 295 fluid density. We will assume that the variance of the rock density is  
 296 0.5% (which is in the lower end of errors reported in core measure-  
 297 ments). In this way we propagate the error in S-wave velocity and  
 298 rock density into the shear modulus; then we propagate the P-wave  
 299 velocity, rock density and shear-modulus variance into the bulk  
 300 modulus. On average, one standard deviation of the estimated P- and  
 301 S-wave travel times is small ( $\hat{\sigma}_t = 0.06 \text{ } \eta\text{s}$ ). Still, a small error in the  
 302 rock density (0.5%) significantly affects the error of the bulk and  
 303 shear moduli estimates ( $\hat{\sigma}_K = 2.4 \text{ GPa}$  and  $\hat{\sigma}_\mu = 0.8 \text{ GPa}$ ) com-  
 304 pared to the errors for data from the stress-strain experiment.

### 305 Frequency averaging

306 Because we acquired data for many frequencies, for the purposes  
 307 of comparison we limit our analysis to 100 Hz which is representa-  
 308 tive of seismic frequency. This distinct frequency value, together  
 309 with the ultrasonic data, gives us estimates of dispersion for the bulk  
 310 and shear moduli. To estimate the rock moduli at 100 Hz, we apply a  
 311 least-squares fit to the logarithm (base 10) of frequency versus Pois-  
 312 son's ratio and Young's modulus for each sample and saturation and  
 313 pick data at 100 Hz. Figure 2 is an example relating the estimated  
 314 (solid line) and measured (symbols) bulk moduli for sample *H*. This  
 315 procedure is only for smoothing purposes. We do not claim that this  
 316 linearity fully describes the dispersion relation.

### 317 VARIATIONS IN SHEAR MODULUS

318 Fluids have a shear modulus of zero, so we expect the dry-or fluid-  
 319 saturated rock shear modulus to be constant (true for many rocks that  
 320 are isotropic and homogeneous). Together with the assumption in  
 321 Gassmann's theory that pore fluids do not chemically alter the me-  
 322 chanical properties of a rock, Gassmann's theory predicts that the  
 323 shear modulus will remain constant under different saturations.  
 324 Thus, a measure of the shear modulus is one way to validate Gas-  
 325 smann's theory.

326 However, our carbonate samples show rock shear modulus  
 327 changes, from dry to brine saturation, of up to 20%. Several labora-  
 328 tory studies have also reported shear modulus changes between 5%  
 329 and 20% from dry to water or brine saturation in carbonates (Vo-  
 330 Thanh, 1995; Assefa et al., 2003; Baechle et al., 2005; Røgen et al.,  
 331 2005; Sharma et al., 2006). The shear modulus of the rock is also sen-  
 332 sitive to small amounts of moisture or partial saturation of water  
 333 (Clark et al., 1984).

334 Rock weakening resulting from fluids has also been observed in  
 335 field data. Water, weakening the rock frame in carbonates, is invoked  
 336 as a primary factor controlling subsidence of the Ekofisk field. Sylte  
 337 et al. (1999) show that compaction of Ekofisk chalks occurs only in  
 338 chalks that are being water flooded. High porosity chalks that have  
 339 original water content (prewater flooding) are not compacting and  
 340 behave elastically throughout the lifetime of the field. They con-  
 341 clude that the injected water weakens invaded chalks resulting in  
 342 compaction and porosity loss. In their study, they compare observa-  
 343 tion to geomechanical models, but do not give the physical-chemical  
 344 mechanisms that could be producing this weakening.

Khazanehdari and Sothcott (2003) compiled rock-fluid interac-  
 tions that explain the rock shear modulus ( $\mu$ ) variability with fluids.  
 They define rock weakening when  $\mu_{\text{saturated}} < \mu_{\text{dry}}$ , and strengthening  
 for  $\mu_{\text{saturated}} > \mu_{\text{dry}}$ . Cardona et al. (2001), based on work from Brown  
 and Korringa (1975) show that for an anisotropic rock, the vertically  
 propagating shear waves are sensitive to the compressibility of the  
 saturating fluid. However, our rocks are largely isotropic at the core  
 scale, although they might be anisotropic at field scale. Therefore, in  
 our work, we will focus on the rock-fluid interactions that are re-  
 sponsible for rock shear modulus changes.

### Data examples of shear modulus sensitivity to fluids and possible explanations

Figure 6 shows the rock shear modulus for sample *C* at seismic  
 and ultrasonic frequencies when dry and brine saturated. Error bars  
 represent one standard deviation of the shear modulus. Two main ob-  
 servations are to be drawn from Figure 6. First, the rock shear modu-  
 lus can either weaken or strengthen upon brine fluid saturation com-  
 pared to the dry rock. At 100 Hz we observe shear modulus weaken-  
 ing from dry to wet, while for 0.8 MHz data the shear modulus  
 strengthens when brine fills the pore space. This implies that more  
 than one rock-fluid mechanism is active.

Second, for the 100 Hz frequency measurements, the shear modu-  
 lus weakens more for low- than for high-differential pressures. Our  
 measurements are performed going from high- to low-differential  
 pressures (unloading cycle). After the experiment with brine satura-  
 tion reached 3.5 MPa, we increased the differential pressure again  
 for three pressure stages (circles in Figure 6). Observe that the rock  
 shear modulus sensitivity to brine saturation for both 100 Hz and  
 0.8 MHz is repeatable; thus, the shear modulus weakening is not af-  
 fected by hysteresis. This reversible weakening or strengthening of  
 the frame is likely associated with the opening and closing of com-  
 pliant pores or cracks. Some of these cracks are intrinsic to the rock,  
 while others might have been induced while drilling or coring. Other  
 samples with significant shear modulus weakening show similar  
 pressure dependence to sample *C*.

Figure 7 compares the dry- and brine-saturated rock shear modu-  
 lus for all samples for 100 Hz at 3.5 and at 31 MPa differential pres-  
 sure. The solid line indicates equal dry- and brine-saturated shear

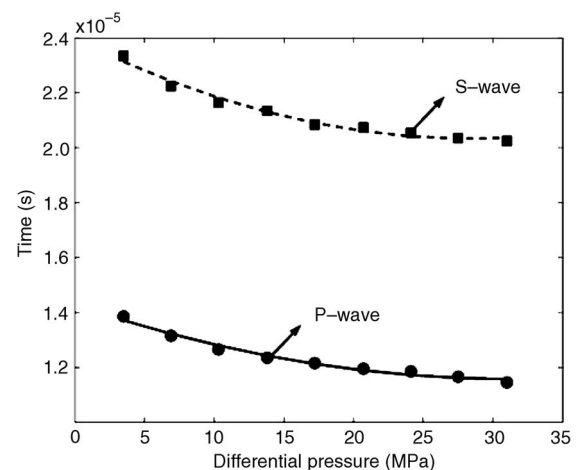


Figure 5. Second-order polynomial fit to ultrasonic travel times as a function of differential pressure for sample *D* under butane saturation.

383 modulus. Most samples have a rock shear modulus around 10 MPa.  
 384 This cluster of data corresponds to samples with high porosity  
 385 (24–35%), while the low-porosity samples have a shear modulus  
 386 larger than 15 MPa. The error bars of the shear modulus (one stan-  
 387 dard deviation) are within the size of the marker. Observe that at low-  
 388 differential pressures (3.5 MPa) all samples show shear modulus  
 389 weakening, while at higher pressures (31 MPa), shear modulus  
 390 weakening is still present but less significantly than for low pressure  
 391 (see also Figure 6).

392 Most samples at ultrasonic frequency and at both 3.5 and 31 MPa  
 393 differential pressure show neither weakening nor strengthening of  
 394 the rock shear modulus within the data uncertainty (Figure 8). Weak-  
 395 ening is observed in samples *B* and *D*, but less than for seismic fre-  
 396 quency (Figure 7).

397 When we compare Figures 7 and 8, the shear modulus for brine-  
 398 saturated rock at ultrasonic frequency is greater than for seismic fre-  
 399 quency. This *comparative* strengthening could describe modulus  
 400 dispersion as a result, for example, of global- and squirt-fluid flow in  
 401 the pore space. However, for samples *B* and *D*, the chemical soften-  
 402 ing of the rock could be dominating over the modulus dispersion. Al-  
 403 ternatively, our ultrasonic-wave velocity represents the fastest path  
 404 (stiffest area in the rock). If the chemical weakening is occurring in  
 405 an isolated area of the sample, the stress-strain experiment measures  
 406 the effective rock deformation (frame softening), while the ultrason-  
 407 ic wave will avoid this area and propagate in the unperturbed rock.

408 We also saturated the carbonate rocks with butane, a highly compress-  
 409 ible, light hydrocarbon (in liquid phase at our elevated pore pres-  
 410 sures). The sensitivity of the rock shear modulus to this fluid is  
 411 much less than for brine (Figure 9).

412 We can now examine what are the possible weakening and  
 413 strengthening mechanisms acting on our carbonate rocks based on  
 414 the work of Khazanehdari and Sothcott (2003). They compiled sev-  
 415 eral mechanisms that can cause the shear modulus to either weaken  
 416 or strengthen when a fluid contacts the solid matrix.

417 Pores and microfractures create surface area in a rock. Surface-

energy reduction (Murphy et al., 1986; Tutuncu and Sharma, 1992) 418  
 and subcritical crack-growth (Atkinson, 1984) mechanisms relate to 419  
 the amount of surface area in a porous rock. Compliant pores and mi- 420  
 crofractures are observed in our samples from thin sections. We also 421  
 know, from the modulus as a function of differential pressure, that 422  
 compliant pores and microfractures open, increasing the surface 423  
 area, as the differential pressure decreases (Figure 6). For our sam- 424  
 ples, open low aspect ratio pores might exhibit growth as well as 425  
 breakage of solid bounds due to interaction with brine. These two 426  
 mechanisms, acting on our carbonate samples, are consistent with 427  
 the fact that a nonpolar fluid, such as butane, saturating the rock, 428  
 does not show significant shear modulus variation (Figure 9). Another 429  
 rock-fluid mechanism such as viscous-coupling (Bourbié et al., 430  
 1987), is probably not the cause of shear modulus variability in car- 431  
 bonates because the sensitivity to brine is large while it is not signifi- 432  
 cant for liquid butane, with both fluids having similar and low vis- 433  
 cosities (0.2 cP for liquid butane and 1 cP for brine). Dissolution of 434  
 carbonate minerals could also be occurring. Dissolution of calcite 435  
 and dolomite minerals depends on the pH of the fluid, temperature, 436  
 and the reaction order of the cations (Ca, Mg, Ba) which control the 437  
 dissolution rate of carbonate minerals (Chou et al., 1989). 438

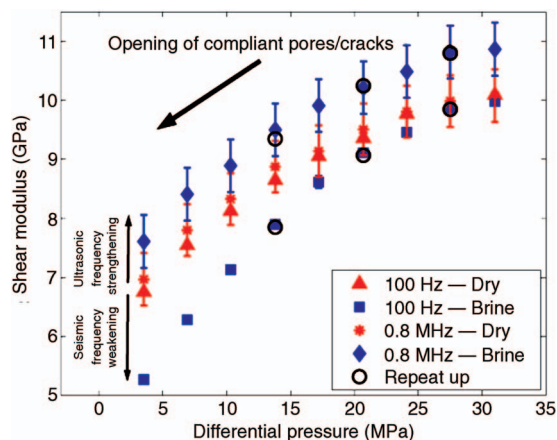


Figure 6. Sample *C*, showing shear modulus weakening and strengthening at seismic and ultrasonic frequencies respectively. Measurements are performed from high- to low-differential pressures. Circles represent repeated differential pressures going from low- to high-differential pressures after the initial unloading cycle was finalized. Note that as we decrease the differential pressure, more compliant pores and cracks open. Error bars are one standard deviation (one  $\sigma$  for seismic frequency data is contained in the size of the symbol).

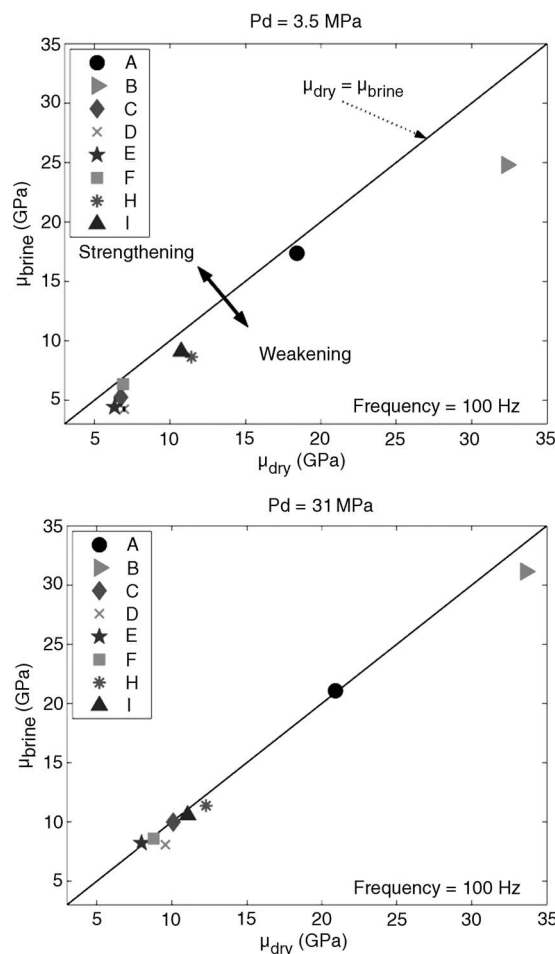


Figure 7. Shear modulus weakening in carbonate samples resulting from dry to brine saturation at seismic frequency (100 Hz) for differential pressures of 3.5 and 31 MPa. Error bars, representing one standard deviation, are within the size of the marker for most samples.

439 By acquiring data at seismic and ultrasonic frequencies, we observe  
 440 evidence of at least three mechanisms for which the shear modulus  
 441 weakens (surface-energy reduction and crack growth) or strengthens (modulus dispersion).  
 442 Changes in shear modulus could be observed from seismic time-lapse data, especially  
 443 in the presence of compliant pores and polar fluids such as water. When injecting  
 444 water into an oil reservoir, the nature of this polar fluid, its viscosity,  
 445 pressure, temperature, etc. will likely interact with the rock solid phases  
 446 creating weakening or strengthening of the shear modulus (and maybe in some cases  
 447 the bulk modulus) compared to the original fluid saturation.  
 448  
 449

450 Also, when logging data is available in a field, the analysis has to  
 451 consider that modulus dispersion can be significant and should be taken with care  
 452 if compared to seismic data. Log data will fall in between our measured frequency  
 453 ranges (~10 KHz). Having knowledge of the characteristic frequency ( $f_c$ ) might help  
 454 the interpretation of log data. The  $f_c$  separates the behavior for relaxed and  
 455 unrelaxed fluids. If  $f_{log} < f_c$  and we have compliant pores, we could observe  
 456 weakening of the shear modulus upon water saturation. On the other hand, if  
 457 the  $f_{log} > f_c$ , strengthening of the shear modulus might be observed. Sharma et al.  
 458 (2006) compiled results for the shear modulus change from dry to water saturation  
 459 from several authors.  
 460

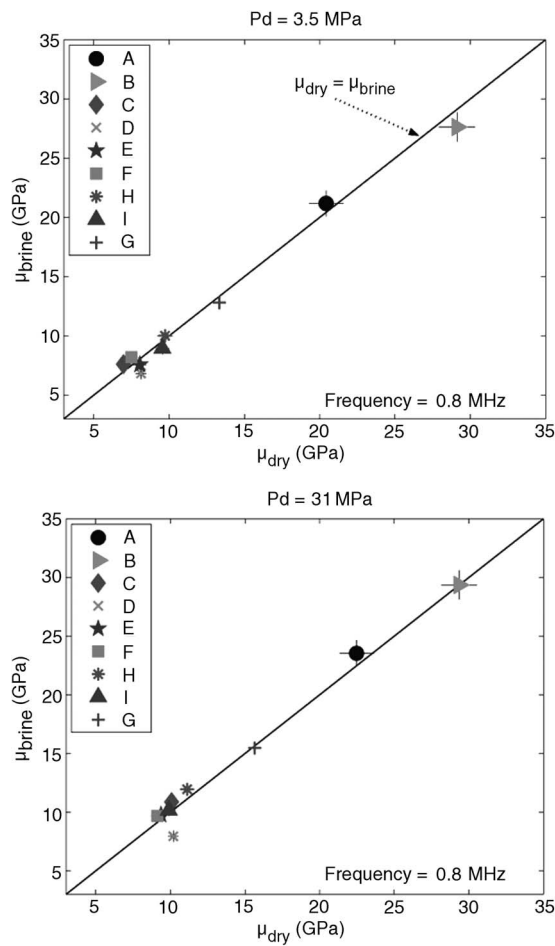


Figure 8. Carbonate samples showing that the shear modulus remains almost constant from dry to brine saturation at ultrasonic frequency for differential pressures of 3.5 and 31 MPa. Error bars, representing one standard deviation, are within the size of the marker for most samples.

In this study, the shear modulus strengthens at ultrasonic frequencies and weakens for sonic frequencies (~10 KHz) for data by Lucet (1989). This observation is in agreement with our observations on shear modulus change from seismic to ultrasonic frequencies.

GASSMANN'S FLUID SUBSTITUTION

We introduced Gassmann's theory with its assumptions, and in this section we compare and analyze the computed saturated bulk modulus, using Gassmann's theory, to the measured rock bulk modulus. Our experimental setting for seismic-frequency data acquisition lets us acquire data when the fluid is at equilibrium. The pore pressure is held constant, thus the fluid modulus is 0.5 GPa for butane, and 3.4 GPa for brine.

Figure 10 compares the bulk modulus, calculated using the Gassmann theory, to the measured bulk modulus for butane-saturated carbonates at frequencies of 100 Hz and 0.8 MHz, and at a differential pressure of 31 MPa. The solid line represents the case where the butane-substituted modulus, predicted by Gassmann's theory, and the measured bulk modulus are equal. Error bars represent one standard deviation for the bulk modulus. Gassmann's theory is correctly pre-

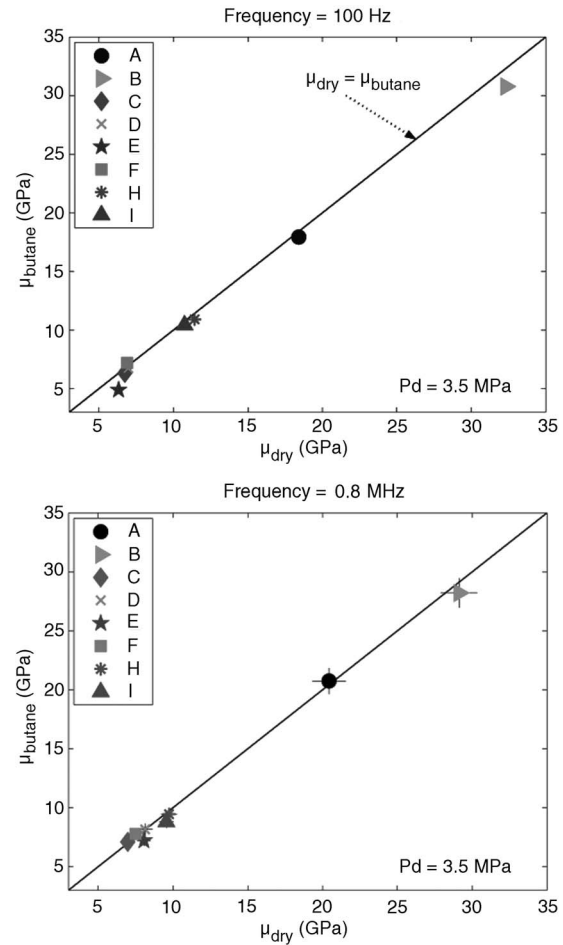


Figure 9. Carbonate samples showing little shear modulus weakening and strengthening resulting from dry to butane saturation compared to the dry-brine saturation case. Both plots are at a differential pressure of 3.5 MPa for seismic and ultrasonic frequencies. Error bars, representing one standard deviation, are within the marker size for most samples.

480 dicting the observed butane-saturated modulus for our carbonate  
 481 samples, partly because the influence of butane on the rock bulk  
 482 modulus is not large. Butane is a highly compressible fluid, thus the  
 483 fluid influence on rock compressibility is not significantly different  
 484 from the dry rock (see Figure 2).

485 For brine saturation, Gassmann-calculated and measured bulk  
 486 moduli  $m$  at 100 Hz and 0.8 MHz, and at differential pressures of 3.5  
 487 and 31 MPa  $m$  are compared in Figures 11 and 12 respectively. The  
 488 solid line represents the case where the fluid-substituted and measured  
 489 moduli are equal. Error bars represent one standard deviation  
 490 for the bulk modulus. Observe that some samples match the predic-  
 491 tions well, while others do not.

492 In Figure 11, at a frequency of 100 Hz, none of the predictions fit  
 493 the observed bulk modulus within the associate uncertainty, while at  
 494 0.8 MHz, for the same differential pressure of 3.5 MPa, the fit to the  
 495 predicted bulk modulus is better. At low-differential pressure and at  
 496 100 Hz, the bulk moduli for all of the samples but  $F$  are overpredic-  
 497 ted by Gassmann's theory. We observe shear modulus weakening for  
 498 all samples (and the least for sample  $F$ , Figure 7), therefore if the  
 499 rock frame has weakened in the presence of brine, so could the bulk  
 500 modulus,  $m$  a factor not accounted for in Gassmann's theory. There-

fore, the overprediction of the bulk modulus by Gassmann's theory  
 at low-differential pressure is probably because the rock frame has  
 been altered (softened).

The bulk modulus is underpredicted for 100 Hz, yet it is well pre-  
 dicted at 0.8 MHz (Figure 11). This is largely a result of modulus  
 dispersion. Remember that Gassmann's theory estimates the saturat-  
 ed modulus for low frequencies. Gassmann's theory uses the bulk  
 modulus of the dry rock, which is not dispersive, to predict the sat-  
 urated rock modulus. However, modulus dispersion exists in most of  
 our brine-saturated carbonates (see Figure 2). This bulk modulus  
 dispersion is evidenced in the shifting of data points in Figure 11 as  
 the frequency increases from 100 Hz to 0.8 MHz. The bulk modulus  
*shift* occurs parallel to the x-axis (measured saturated bulk modu-  
 lus). This bulk modulus dispersion at ultrasonic frequency can lead  
 to errors when comparing ultrasonic to seismic data. Thus, a better fit  
 at ultrasonic frequency might be somewhat of a paradox on Gas-  
 smann's-theory applicability for carbonates.

At a differential pressure of 31 MPa (Figure 12), the 100 Hz data  
 shows that the bulk modulus of four brine-saturated carbonates ( $B$ ,  
 $E$ ,  $I$ , and  $H$ ) is predicted well by Gassmann's theory. The bulk moduli  
 for samples  $A$  and  $C$  are largely overpredicted by Gassmann's theo-

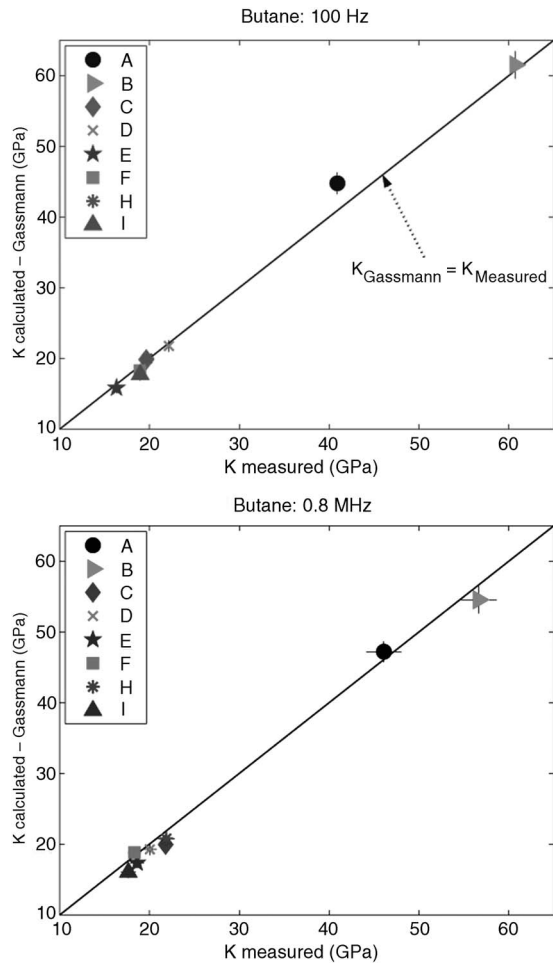


Figure 10. Butane-saturated bulk moduli measured and estimated with Gassmann's theory for 100 Hz and 0.8 MHz at 31 MPa differential pressure. Solid line represents equal measured and estimated bulk modulus. Error bars are one standard deviation of the bulk modulus.

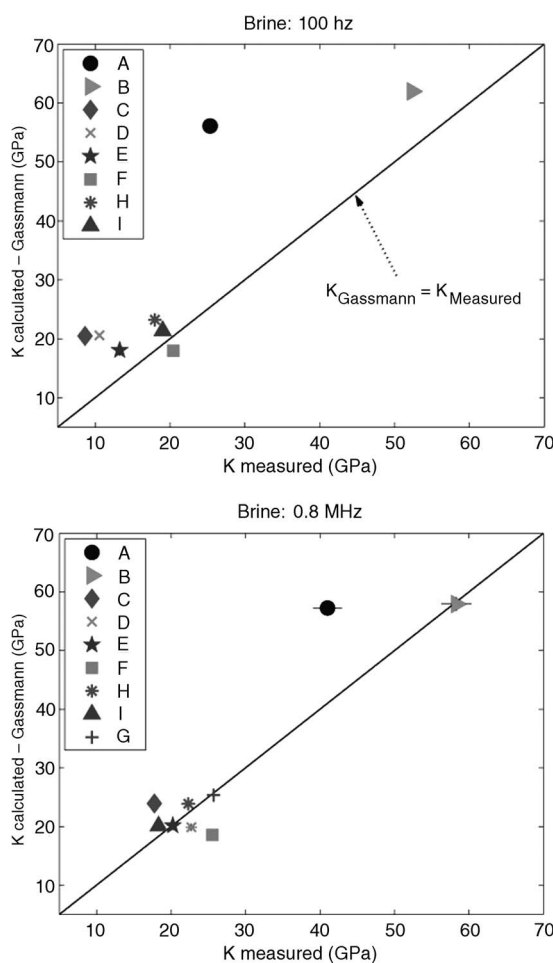


Figure 11. Brine-saturated bulk moduli measured and estimated with Gassmann's theory for 100 Hz and 0.8 MHz at 3.5 MPa differential pressure. Solid line represents equal measured and estimated bulk modulus. Error bars are one standard deviation of the bulk modulus.

522 ry. Samples *A* and *C* have the highest content of non-calcareous min- 543  
 523 erals, especially clay. We ignore that softening of clays is a possible 544  
 524 mechanism for elastic moduli weakening for most of our samples. 545  
 525 However, that  $K_{Measured}$  is significantly less than  $K_{Gassmann}$  for samples 546  
 526 *A* and *C* is possibly related to frame (clay) weakening in the presence 547  
 527 of brine.

528 We focus now on data at 100 Hz, where frequencies are low 548  
 529 enough that we expect the fluid-pressure gradients are zero, as Gas- 549  
 530 ssmann's theory requires. Still, at high differential pressure, we ob- 550  
 531 serve that some samples are well predicted by Gassmann's theory, 551  
 532 while others are not. So where can this difference come from? On 552  
 533 one hand, we have observed rock shear modulus sensitivity to brine 553  
 534 saturation. On the other hand, for low-differential pressures, we ex- 554  
 535 pect to have open compliant pores or cracks. Gassmann's equations 555  
 536 are derived without assuming any specific pore geometry, and can be 556  
 537 applied to any pore type as long as the assumptions for Gassmann's 557  
 538 theory are satisfied, i.e. pore pressure is in equilibrium. The mis- 558  
 539 match between observed and Gassmann-predicted bulk modulus 559  
 540 could relate to differences in pore type creating pressure gradients or 560  
 541 chemical reactions which violate Gassmann's assumptions. There- 561  
 542 fore, samples yielding better predictions by Gassmann's theory

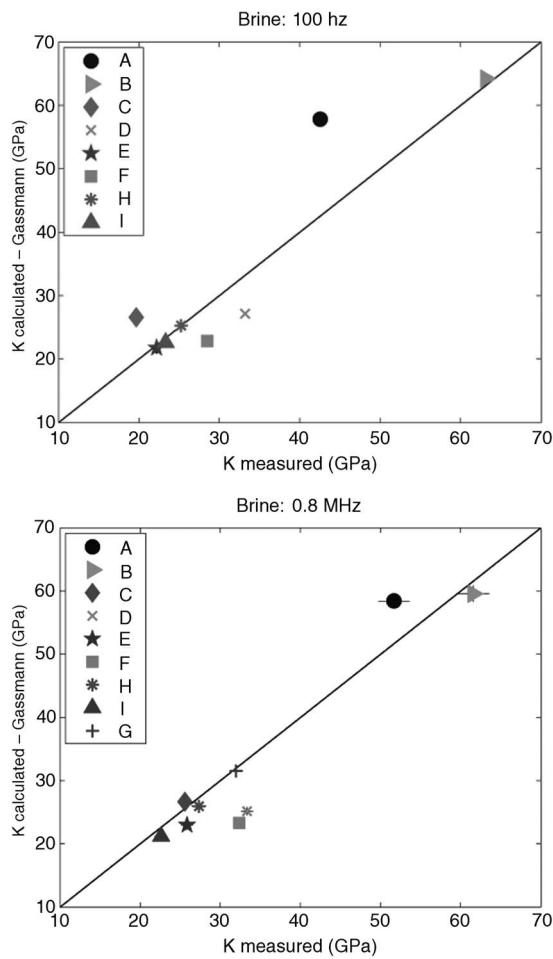


Figure 12. Brine-saturated bulk moduli measured and estimated with Gassmann's theory for 100 Hz and 0.8 MHz at 31 MPa differential pressure. Solid line represents equal measured and estimated bulk moduli. Error bars are one standard deviation of the bulk modulus.

543 might be explained through the dependence of bulk modulus with 544  
 545 differential pressure. Figure 13 plots the bulk modulus of brine-satu- 546  
 547 rated carbonates as a function of differential pressure. The anom- 548  
 549 alous behavior of sample *D* at 20.7 MPa is due to a small gas leak into 549  
 550 the rock when the sample was saturated with brine. This dramati- 550  
 551 cally lowered the bulk modulus of sample *D* at low frequencies for pres- 551  
 552 sures lower than 20.7 MPa. In Figure 13, we observe a consistent 552  
 553 linear behavior of the bulk modulus with differential pressure from 553  
 554 the Hertz-Mindlin model:  $K = mP^{1/3}$  (Mavko et al., 1998), where the 554  
 555 slopes ( $m$ ) of the linear trends are different for different rocks. High- 555  
 556 er slopes mean larger dependence on differential pressure, indicat- 556  
 557 ing the existence of compliant pores or microcracks. Table 2 com- 557  
 558 pares Gassmann's predictability, shear modulus weakening, miner- 558  
 559 alogy, and pressure effect on all samples at 100 Hz. Gassmann's pre- 559  
 560 dictability and shear modulus weakening are reported for the highest 560  
 561 differential pressure reached at 31 MPa. The pressure effect is mea- 561  
 562 sured by the slope of the linear dependence ( $m$ ) of the bulk modulus 562  
 563 (Figure 13). 563

564 There seems to be no correlation between the shear modulus 564  
 565 weakening and the observed match between measured and comput- 565  
 566 ed bulk moduli for brine-saturated carbonates at high differential 566  
 567 pressure (Table 2). For example, both samples *B* and *D* show signifi- 567  
 568 cant shear modulus weakening at 31 MPa differential pressure; still 568  
 569 sample *B* is well predicted by Gassmann's theory while sample *D* is 569  
 570 not. It might seem confusing that although Gassmann's assumption 570  
 571 that the rock frame stays unaltered by the fluid is violated for some 571  
 572 samples, the measured brine-saturated bulk modulus is well predict- 572  
 573 ed by Gassmann's theory for these samples. A likely reason for this 573  
 574 is because the increase in bulk modulus, in absolute percent from dry 574  
 575 to brine saturation (35% in average), is more significant than the shear 575  
 576 modulus weakening, in absolute percent (6% in average). 576

577 Examining the pressure dependence, the saturated bulk modulus 577  
 578 for samples with lower slopes (*B*, *E*, *H* and *I*) is well predicted by 578  
 579 Gassmann's theory. Low slopes mean the sample has less compliant 579  
 580 pores or cracks. Samples *A*, *C* and *D* have high slopes, and Gas- 580  
 581 ssmann's theory is not predicting the observed saturated bulk mod- 581  
 582 ulus. Sample *F* has an intermediate slope, but the saturated bulk 582  
 583 modulus is not well predicted by Gassmann's theory. For sample *F*, 583  
 584 the bulk modulus as a function of pressure is less smooth than for other 584  
 585 samples, leading to a higher variance in the slope calculation. As pre-

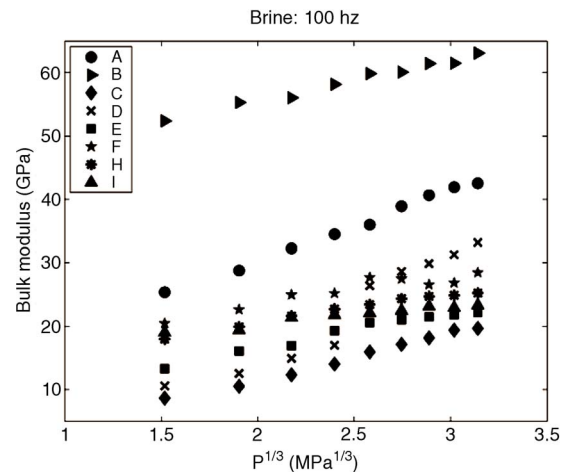


Figure 13. Bulk modulus for carbonates with brine saturation as a function of differential pressure ( $P^{1/3}$ ) for 100 Hz.

**Table 2. Gassmann's theory applicability correlated with shear-modulus weakening and bulk-modulus dependence with pressure (slopes of Figure 13). Gassmann and shear-modulus analysis corresponds to 100 Hz at a differential pressure of 31 MPa. X means the statement is true. Dominant mineralogy: C=calcite, D=dolomite. Note correspondence of good Gassmann's theory fit with low-pressure dependence (*m*).**

| SAMPLES                                | A    | B   | C   | D    | E   | F   | H   | I   |
|--|------|-----|-----|------|-----|-----|-----|-----|
| Gassmann's theory fits                 |      | X   |     |      | X   |     | X   | X   |
| Shear modulus weakening                |      | X   |     | X    |     |     | X   |     |
| Bulk modulus vs. pressure ( <i>m</i> ) | 11.8 | 5.6 | 7.9 | 11.2 | 5.2 | 5.4 | 4.5 | 3.2 |
| Mineralogy                             | C    | D   | C   | C    | C   | C   | D   | D   |

583 viously mentioned, our experimental setup could not quite reach the  
 584 differential pressure of the reservoir at 34.5 MPa. This could result  
 585 in some compliant pores still being open at these pressures. From  
 586 this we conclude that open compliant pores are a possible factor af-  
 587 fecting the mismatch between observed and predicted bulk modulus.  
 588 Samples *B*, *H* and *I* are dolomites, but we do not have enough statisti-  
 589 cal data to make correlations with rock grain density. Nevertheless,  
 590 these dolomite samples have high porosity and permeability *m* prob-  
 591 ably satisfying Gassmann's assumption on pore connectivity and  
 592 fluid distribution in the porous space.

593 From our observations, carbonates with round pores, vugs or mi-  
 594 critic textures are well predicted by Gassmann's theory for low fre-  
 595 quencies. Even at reservoir pressures, open compliant pores or  
 596 cracks might be present at reservoir in-situ conditions. In this case,  
 597 an anisotropic fluid-substitution theory, such as that of Brown and  
 598 Korringa (1975), is perhaps more appropriate. However, knowledge  
 599 of the anisotropic symmetry, with all of the stiffness coefficients of  
 600 the rock and the pore-space compressibility, are required for this the-  
 601 ory. Using additional parameters might allow one to fit the data bet-  
 602 ter, but the estimated parameter could not be realistic or representa-  
 603 tive of the rock.

604 **CONCLUSIONS**

605 We present data over a large range of frequencies and under vary-  
 606 ing saturation and pressure conditions to investigate the applicabili-  
 607 ty of Gassmann's theory for our carbonate data set. We observe that  
 608 the rock shear modulus is sensitive to brine saturation, especially at  
 609 seismic frequencies. Weakening of the solid matrix occurs possibly  
 610 due to surface energy loss and/or subcritical crack growth in compli-  
 611 ant pores, mostly at low-differential pressures. These mechanisms  
 612 violate an assumption of Gassmann's theory that the fluid does not  
 613 influence the solid matrix of the rock. However, we find no positive  
 614 correlation between the rock shear modulus weakening and the fail-  
 615 ure of Gassmann's theory to predict the saturated bulk modulus at  
 616 seismic frequencies. We do find that the brine-saturated bulk modu-  
 617 lus, for carbonates with small differential pressure dependence  
 618 (round pores or vugs), is well predicted by Gassmann at seismic fre-  
 619 quencies, while for carbonates strongly influenced by pressure  
 620 (compliant pores or microcracks), Gassmann's theory does not  
 621 match the observations. Therefore, knowledge of the reservoir pore-

space geometry can aid in the understanding and applicability of  
 Gassmann's theory.

Predicting the saturated bulk modulus at ultrasonic frequencies  
 violates Gassmann's low-frequency assumption. Nevertheless, we  
 test our carbonate samples at ultrasonic frequencies to show the role  
 of modulus dispersion. For some of our samples, the measured and  
 Gassmann-calculated bulk moduli at ultrasonic frequencies show  
 better agreement compared to seismic frequencies. This match is ap-  
 parent, resulting from bulk modulus dispersion which we observe in  
 our carbonates when saturated with brine. We also observe shear  
 modulus dispersion. Little change from dry to brine saturation is  
 present in the rock shear modulus at ultrasonic frequencies, but this  
 modulus is always higher than the shear modulus obtained at seismic  
 frequencies. This increase could be a result of dispersion or a prefer-  
 ential propagation path, which avoids altered (weakened) sections in  
 the saturated rocks. Although our conclusions are based on samples  
 with different texture and mineralogy, we must be careful to general-  
 ize these results to all carbonate rocks.

Our observations are applicable particularly to the analysis of  
 time-lapse data. Ultrasonic laboratory data is used in some cases to  
 calibrate time-lapse seismic reflection data. We should be aware that  
 bulk modulus in carbonate rocks can have significant dispersion af-  
 fecting the applicability of Gassmann's fluid-substitution theory at  
 ultrasonic frequencies (and maybe at log frequencies). Also, when  
 water or brine replaces a nonpolar fluid such as oil, shear modulus  
 weakening can be observed in the field. Brine of different salinity  
 and temperature injected in an aquifer to enhance production might  
 change the solid frame, causing variation in the moduli of the rocks.

**ACKNOWLEDGMENTS**

We would like to thank Statoil for providing the cores and useful  
 discussions. We also thank De-Hua Han for measuring sample *G* at  
 ultrasonic frequencies and K/T GeoServices Inc. for the XRD analy-  
 sis. We would like to thank Kasper van Wijk, as well as Ronny Hof-  
 mann, Manika Prasad, Martin Landrø, Luis Tenorio, John Scales,  
 Thomas Davis and Dave Hale, for their feedback and discussions.  
 We also thank the support of all of the members of the Fluid and DHI  
 Consortia.

**REFERENCES**

Anselmetti, F. S., and G. P. Eberli, 1993, Controls on sonic velocity in car-  
 bonates: Pure and Applied Geophysics, **141**, 287–323.  
 Assefa, S., C. McCann, and J. Sothcott, 2003, Velocities of compressional  
 and shear waves in limestones: Geophysical Prospecting, **51**, 11–13.  
 Atkinson, B. K., 1984, Subcritical crack growth in geological materials:  
 Journal of Geophysical Research, **89**, 4077–4114.  
 Baechle, G. T., R. J. Weger, G. P. Eberli, J. L. Massafarro, and Y.-F. Sun,  
 2005, Changes of shear moduli in carbonate rocks: Implications for Gas-  
 smann applicability: The Leading Edge, **24**, 507–510.  
 Batzle, M. L., D.-H. Han, and R. Hofmann, 2006, Fluid mobility and fre-  
 quency-dependent seismic velocity: Direct measurements: Geophysics,  
**71**, N1–N9.  
 Berryman, J. G., 1999, Origin of Gassmann's equations: Geophysics, **64**,  
 1627–1629.  
 Biot, M. A., 1956, Theory of propagation of elastic waves in a fluid-saturated  
 porous solid. I. Low-frequency range: The Journal of the Acoustical Soci-  
 ety of America, **28**, 168–178.  
 Birch, F., 1960, The velocity of compressional waves in rocks to 10 kilobars,  
 Part 1: Journal of Geophysical Research, **65**, 1083–1102.  
 Bourbié, T., O. Coussy, and B. Zinszner, 1987, Acoustics of porous media:  
 Gulf Publishing Company.  
 Brown, R., and J. Korringa, 1975, On the dependence of the elastic properties  
 of a porous rock on the compressibility of the pore fluid: Geophysics, **40**,  
 608–616.

- 684 Cardona, R., M. Batzle, and T. L. Davis, 2001, Shear wave velocity dependence on fluid saturation: SEG Technical Program, Expanded Abstracts, 1712–1715. 721
- 685 Chou, L., R. M. Garrels, and R. Wollast, 1989, Comparative study of the kinetics and mechanisms of dissolution of carbonate minerals: *Chemical Geology*, **78**, 269–282. 722
- 686 Clark, V. A., B. R. Tittmann, and T. W. Spencer, 1984, Rock lithology and porosity determination from shear and compressional wave velocity: *Geophysics*, **49**, 1188–1195. 723
- 687 Domenico, S. N., 1984, Rock lithology and porosity determination from shear and compressional wave velocity: *Geophysics*, **49**, 1188–1195. 724
- 688 Dutta, N. C., and H. Ode, 1979, Attenuation and dispersion of compressional waves in fluid-filled porous rocks with partial gas saturation (White model): Part II: Results: *Geophysics*, **44**, 1789–1805. 725
- 689 Gassmann, F., 1951, Über die elastizität poröser medien: *Vierteljahrsschrift der Naturforschenden Gesellschaft in Zürich*, **96**, 23. 726
- 690 Han, D.-H., 2004, Velocity in carbonate rocks: Fluids and DHI Consortia Sponsor Meeting, Technical Report. 727
- 691 Hudson, J. A., 1981, Wave speeds and attenuation of elastic waves in material containing cracks: *Geophysical Journal of the Royal Astronomical Society*, **64**, 133–150. 728
- 692 Khazanehdari, J., and J. Sothcott, 2003, Variation in dynamic elastic shear modulus of sandstone upon fluid saturation and substitution: *Geophysics*, **68**, 472–481. 729
- 693 Kuster, G. T., and M. N. Toksoz, 1974, Velocity and attenuation of seismic waves in two-phase media: Part I. Theoretical formulations: *Geophysics*, **39**, 587–606. 730
- 694 Lucet, N., 1989, Vitesse et atténuation des ondes élastiques soniques et ultrasoniques dans les roches sous pression de confinement: Ph.D. thesis, L'Université de Paris. 731
- 695 Marion, D., and D. Jizba, 1997, Acoustic properties of carbonate rocks: Use in quantitative interpretation of sonic and seismic measurements in I. Palaz, and K. J. Marfurt, eds., *Carbonate Seismology*: SEG, 75–93. 732
- 696 Mavko, G., and D. Jizba, 1991, Estimating grain-scale fluid defects on velocity dispersion in rocks: *Geophysics*, **56**, 1940–1949. 733
- 697 Mavko, G., T. Mukerji, and J. Dvorkin, 1998, *The rock physics handbook*: Cambridge University Press. 734
- 698 Moore, C. H., 2001, Carbonate reservoirs: Porosity evolution and diagenesis in a sequence stratigraphic framework: *Developments in Sedimentology*: Elsevier Science Publishing Company, Inc. 735
- 699 Murphy, W. F., K. W. Winkler, and R. L. Kleinberg, 1986, Acoustics relaxation in sedimentary rocks: Dependence on grain contacts and fluid saturation: *Geophysics*, **51**, 757–766. 736
- 700 O'Connell, R. J., and B. Budiansky, 1974, Stress-induced velocities in dry and saturated cracked solids: *Journal of Geophysical Research*, **79**, 4626–4627. 737
- 701 Røgen, B., I. L. Fabricius, P. Japsen, C. Høier, G. Mavko, and J. M. Pedersen, 2005, Ultrasonic velocities of North Sea chalk samples: Influence of porosity, fluid content and texture: *Geophysical Prospecting*, **53**, 481–496. 738
- 702 Sharma, R., M. Prasad, G. C. Katiyar, and G. Surve, 2006, In the applicability of Gassmann model in carbonates: Society of Petroleum Geophysicists Conference, India. 739
- 703 Spencer, J. W., 1981, Stress relaxation at low frequencies in fluid saturated rocks: Attenuation and modulus dispersion: *Journal of Geophysical Research*, **86**, 1803–1812. 740
- 704 Sylte, J. E., L. K. Thomas, D. W. Rhett, D. D. Bruning, and N. B. Nagel, 1999, Water induced compaction in the Ekofisk field: Society of Petroleum Engineers Annual Technical Conference, SPE 56426. 741
- 705 Tutuncu, A. N., and M. M. Sharma, 1992, The influence of fluids on grain contact stiffness and frame moduli in sedimentary rocks: *Geophysics*, **57**, 1571–1582. 742
- 706 Vo-Thanh, D., 1995, Influence of fluid chemistry on shear-wave attenuation and velocity in sedimentary rocks: *Geophysical Journal International*, **121**, 737–749. 743
- 707 Wang, Z., W. K. Hirsche, and G. Sedgwick, 1991, Seismic monitoring of water floods? — A petrophysical study: *Geophysics*, **56**, 1614–1623. 744
- 708 Wang, Z., 1997, Seismic properties of carbonate rocks in I. Palaz, and K. J. Marfurt, eds., *Carbonate Seismology*: SEG, 29–52. 745
- 709 Wang, Z., 2000, The Gassmann equation revised: Comparing laboratory data with Gassmann's predictions in Z. Wang, A. Nur, and D. A. Ebrum, eds., *Seismic and Acoustic Velocities in Reservoir Rocks*: SEG, 8–23. 746
- 710 White, J. E., 1975, Computed seismic speeds and attenuation in rocks with partial gas saturation: *Geophysics*, **40**, 224–232. 747
- 711 748
- 712 749
- 713 750
- 714 751
- 715 752
- 716 753
- 717 754
- 718 755
- 719 756
- 720